Materials Science and Engineering C 73 (2017) 417–424

Contents lists available at ScienceDirect

Materials Science and Engineering C

journal homepage: www.elsevier.com/locate/msec

Immobilization of glucose oxidase onto a novel platform based on modified TiO_2 and graphene oxide, direct electrochemistry, catalytic and photocatalytic activity

Nasibeh Haghighi [a], Rahman Hallaj [a,b,*], Abdollah Salimi [a,b]

[a] Department of Chemistry, University of Kurdistan, P.O. Box 416, Sanandaj, Iran
[b] Nanotechnology Research Center, University of Kurdistan, P.O. Box 416, Sanandaj, Iran

ARTICLE INFO

Article history:
Received 25 September 2016
Received in revised form 9 November 2016
Accepted 4 December 2016
Available online 11 December 2016

Keywords:
Titanium oxide
Glucose oxidase
Electrodeposition
Biosensor
Photocatalytic

ABSTRACT

In this work a new organic–inorganic nanocomposite has been introduced for enzyme immobilization. The composite consisting of graphene oxide (GO) and titanium oxide nanoparticles (TiO_2) modified with 2, 2′-dithioxo-3, 3′-bis (3-(triethoxysilyl) propyl)-2H, 2′H-[5, 5′-bithiazolylidene]-4, 4′(3H, 3′H)-dione as Organic-Inorganic Supporting Ligand (OISL). The OISL was covalently attached to TiO_2 nanoparticles and employed for obtaining a suitable solid surface to enzyme attachment. The glucose oxidase (GOD) was irreversibly loaded on the GC/GO/TiO_2-OISL using consecutive cyclic voltammetry. The enzyme immobilization and the enzymatic activity were determined by electrochemical methods. The cyclic voltammogram displayed a pair of well-defined and nearly symmetric redox peaks with a formal potential of −0.465 V and an apparent electron transfer rate constant of 1.74 s^{-1}. The GO/TiO_2-OISL can catalyze the electroreduction and electrooxidation of hydrogen peroxide. The GC/GO/TiO_2-OISL/GOD electrode was used in the hydrogen peroxide determination. The fabricated nanobiocomposite shows dramatic photoelectrocatalytic activity which evaluated by studying the electrocatalytic activity of the fabricated electrode toward hydrogen peroxide in darkness and in the presences of light.

1. Introduction

Enzymes are important components of electrochemical probes due to their selectivity for catalysis and sensors. As the redox center has been buried in the biological matrix deeply the electrochemical communication between the electro-active groups of redox proteins and electrode surface is very difficult. On the other hand, activity and stability of loaded enzyme are extremely affected by using materials and their surfaces and immobilization strategies. Most of the surfaces tend to denature enzyme structures, therefore, direct electron transfer between enzymes and electrodes is rare and typically their rates are slow. The use of different nanostructures has been demonstrated as an excellent surface and a transducer to enzyme loading. As a consequence of their unique physical, chemical, large surface area, good adsorption capacity electrical, catalytic and optical properties and biocompatibility, nanostructures materials have been developed for immobilization of enzymes [1]. Within last two decades, thousands of reports have been published on different nanostructures materials and their applications. Various types of nanoparticles [2], nano-pores [3], nanotubes [4], nanowires [5], nano-fibers [6], and quantum dots [7] have been used in immobilization of enzymes and biomolecules. Modification of the unfavorable orientation is one of the effective approaches to facilitation of direct electron transfer between the electroactive centers inside redox protein structures and the electrode surfaces [8]. Enzyme immobilization has been always a critical step to employ the enzymes as an industrial biocatalyst. Many researchers have endeavored to improvement of enzyme properties during the immobilization process [9–11]. In addition, simultaneous immobilization and purification of enzymes without sacrificing activities, is very important in the functionalization and immobilization protocol [12–14]. It is well known that only after several enzymes–support interactions, the active site successfully keeps the loaded enzyme under the immobilization conditions. In fact, the multipoint attachment is the critical key to improve enzyme stableness with a better orientation [15,16]. On the other hand, the immobilization mechanism on the various supports may open new strategies to reach this purpose. Several metal multiporous film oxides, such as cobalt oxide [17], zinc oxide [18], nickel oxide [19], iron oxide [20], and titanium oxide [21] have been investigated in the respect of biomolecule electrode interactions. Owing to the inherent advantages of the TiO_2 nanomaterials, including biocompatibility, large surface area, low cost, high photocatalytic and electrocatalytic activity, TiO_2 nanomaterials are favorable and have been used to construct a large variety of novel

* Corresponding author at: Department of Chemistry, University of Kurdistan, P.O. Box 416, Sanandaj, Iran.
E-mail addresses: Haghighi.nasibeh@yahoo.com (N. Haghighi), Rhallaj@uok.ac.ir (R. Hallaj).

http://dx.doi.org/10.1016/j.msec.2016.12.015
0928-4931/

catalysis and photocatalysis based devices and electrochemical sensors and biosensors [22]. Direct electrochemistry of several biomolecules and enzymes such as hemoglobin [23], glucose oxidase (GOD) [24–26] horse radish peroxidase (HRP) [27], cytochrome C [28,29] were studied onto the surface of TiO_2 nanostructures as a supporting material. It has been proven that the modification of TiO_2 on the electrode could enhance the enzyme catalytic performance for promising biosensor applications [30,31]. Furthermore, different organic and inorganic materials used in surface modification of nanostructures, because, it's obvious that, the interaction between supporting materials and biomolecules have been considered for successive loading, and their corresponding performance. Numerous ways have been investigated aiming the loading and shortening of the distance between the enzyme redox sites and the electron transfer mediator [32–34]. It is well known that immobilization strategies of enzymes have a critical role in enzyme activities and enzymatic biosensors stability. These immobilization strategies are based on biospecific interactions, cross-linking and covalent attachments used in enzyme immobilization [35,36]. Repetitive cyclic voltammetry used as an effective protocol for enzyme loading. This strategy could be help to coupling the functional group and alignment the enzyme molecules onto the electrode surface [37]. of structure, biological activity of enzymes, and their functions extremely corresponded to loading methods. Therefore; the ability to adjust the surface properties and surface modifications to match the biomolecules and support for anchoring electrochemically active compounds onto electrode surfaces is very important. Various functional materials are widely used to the specific immobilization of enzymes through their functional groups and multipoint attachment. For example, surface modification of antibacterial TiO_2/Ag^+ nanoparticles by grafting, g-aminopropyltriethoxy silane [22], surface treatment of titanium dioxide (TiO_2) powder using methacryloxy propyltrimethoxy silane [38] and adsorption of 1, 10-bis (4-carboxybenzyl)-4, 40-bipyridinium dibromide compound ($H_2BpybcBr_2$) onto the surface of a nanocrystalline TiO_2 [39] were reported previously. In this work a new organic-inorganic supporting material was prepared and used in immobilization of GOD onto TiO_2 nanoparticles. The remains of immobilized GOD activity are essential for direct electrochemistry, which is evaluated by electrochemical and spectroscopic methods. Direct electron transfer at the surface of bio-electrode is of great interest in both fundamental knowledge of the redox proteins behaviour and the development of novel biosensors and biofuel and bio-electronic devices [40].

2. Experimental details

2.1. Chemicals and apparatus

Anatase titanium oxide (TiO_2) nano-powder, with average particle size of 15–20 nm, was commercially purchased from MTI Corporation. Glucose oxidase (GOD) was purchased from Sigma and used without further purification. The buffer solutions (0.05 M) were prepared form of H_3PO_4, KH_2PO_4 and K_2HPO_4 and adjusting the pH were regulated with HCl and KOH solutions. H_2O_2 (30%w/w) was from Merck, its diluted solution was prepared daily. All solutions were prepared with double distillated water. Pure N_2 was passed through the solution to avoid possible oxygen action during the experiments. Carry 1A UV–vis spectrometer (Perkin-Elmer instruments) has been used to record the Ultraviolet and visible (UV–vis) absorption spectra on an ITO glass electrode. A mira3-Tesacn electron microscope was used in imaging and morphological studies of the surface. Electrochemical experiments were performed with a computer controlled μ-Autolab modular electrochemical system (Eco Chemie Ultecht, The Netherlands), driven by GPES software (Eco Chemie). Also a typical three-electrode cell using an SCE (sat KCl) as a reference electrode, a Pt wire as a counter electrode and a glassy carbon disk as a working electrode was used. All experiments were carried out at ambient temperature.

2.2. Preparation of organic-inorganic support ligand

Organic-inorganic supporting ligand (OISL) was synthesized by following procedure [41]. To a stirred solution of carbon disulfide (0.36 g, 4.8 mmol) and dimethyl acetylene dicarboxylate (0.28 g, 2 mmol) was added drop wised 3-(triethoxysilyl) propan-1-amine (0.88 g, 4 mmol) in 5 min. The reaction mixture was allowed to stir for 2 min. After completion, the addition of EtOH to the reaction mixture generates product as orange crystals. M.p: 330 °C (decompose).

2.3. Preparation of GC/GO/TiO_2-IOSL

The graphene oxide was prepared according to a modified Hummers method [43–44].

Briefly, first 5.0 g natural graphite powder and 2.5 g of sodium nitrate were mixed in 115 ml of concentrated sulphuric acid, and the mixture was cooled to 0–5 °C using ice bath. The mixture was stirred for 30 min at the same temperature and 15 g potassium permanganate was added very slowly. Then the mixture was stirred at 35 °C for 30 min. The resulting solution was diluted by adding 230 ml of water. After this step the color has changed to brown and the reaction temperature rapidly reached to 98 °C. After 15 min the mixture cooled with water-bath for 15 min and the reaction mixture was diluted with 500 ml of water and treated 5 ml of hydrogen peroxide (30%). After air cooling, the mixture was purified by filtration, and multiple rinsing with 10% hydrochloric acid and then the deionized water, centrifugations, and decanting followed by a final vacuum drying. The inorganic-organic nanocomposites were prepared as following procedure. At first, 10 mg of dried TiO_2 nanoparticles, dispersed in 2 ml of ethanol solution which contained 1% of IOSL, with the aid of sonication for 1 h. The excess of IOSL was removed by successive washing with ethanol. Next, after discarding the supernatant, modified nanoparticles were washed by centrifugation with ethanol for three times [42]. The TiO_2-IOSL nanocomposite dispersed in ethanol and sonicated for 30 min. 10 μL of resulting mixture was casted onto a glassy carbon electrode (GC) in preparation of GC/GO/TiO_2-IOSL and subsequently used in immobilization of Glucose Oxidase. Surface modification of TiO_2 nanoparticles showed in Fig. 1 schematically.

2.4. Enzyme immobilization on the TiO_2-IOSL

The high surface area and a large number of functional groups on TiO_2-IOSL are good matrixes for the immobilization of enzymes. The fabricated GC/GO/TiO_2/films were dried at 50 °C under vacuum for 2 h. Next repetitive cyclic voltammetry has been used for immobilization of glucose oxidase onto nanocomposite films. The electrode was immersed in fresh phosphate solution containing 5 mg ml^{-1} glucose oxidase and the potential was repetitively cycled (30 scans) from 1.0 to −1.0 V at scan rate 50 mVs^{-1}. Finally, the modified electrode was removed from enzyme solution, washed with deionized water, and stored at refrigerator temperature (4 °C) before being used in experiments. Recorded cyclic voltamograms of the GC/GO/TiO_2 in 0.07 M fresh phosphate buffer solution (pH = 7.4) containing 5 mM of glucose oxidase depicted in Fig. 2. As shown the well-known redox couple corresponded to glucose oxidase was displayed after a few scans and was grown during the cycling, indicating the glucose oxidase loading onto the GC/GO/TiO_2-IOSL-electrode. The electrochemical properties of GC/GO/TiO_2-IOSL/GOD were evaluated subsequently.

3. Results and discussions

3.1. Characterization of TiO_2-IOSL

The new synthesized organic-inorganic modified TiO_2 shows very distinctive characteristics.

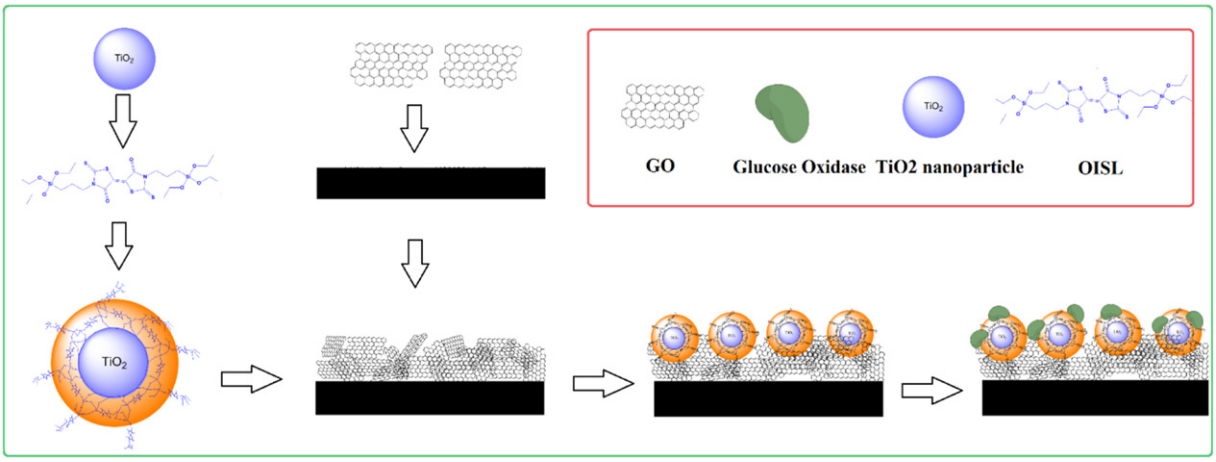

Fig. 1. Schematic fabrication of GC/GO/TiO_2-IOSL/GOD nanocomposite.

Field-emission scanning electron microscopy (FE-SEM) shows graphene nano-sheets (Fig. 3A) and uniform modified nanoparticles with a diameter of 15–20 nm (Fig. 3B), aggregated heavily. The graphene oxide helps to the construction of porous and uniform nanocomposite with lower degree of aggregations. As can be seen (Fig. 3C) GO/TiO_2-IOSL nanocomposite is composed of graphene nanosheets and nanoparticles. These nanoparticles appear to anchor on the surface of the graphene nanosheet. Fig. 3 D&E shows the TEM image and the XRD pattern of prepared graphene respectively. The diffraction pattern shows obviously, the peak at $2\theta = 10.6$ which related to the (001) reflection of graphene oxide, typically. The FTIR spectroscopy is considered to be used in confirmation of condensation reaction between the ethoxy group in IOSL and the TiO_2 surface hydroxyl group. Fig. 4 shows FTIR spectra of alone IOSL, TiO_2-IOSL and unmodified TiO_2 nano-particles. The bands which assigned to alkyl groups [–(CH2)n–] are shown at region 2920 and 2850 cm^{-1} and a Stretch vibration band of Ti–O–Si, appeared in the spectrum around 928 cm^{-1} [45,46]. Also, O–Si asymmetric flexible vibration and main characteristic peaks of Si–O–C bonds shown in 1000–1300 cm^{-1} and 1455–1555 cm^{-1} respectively [46]. These results implied in successful modification of TiO_2 nanoparticles whit IOSL.

3.2. Characterization of GC/TiO_2-IOSL/GOD

As a powerful tool, electrochemical impedance spectroscopy was used in characterization of interface properties of the modified surface of an electrode. It allows following the surface coverage, deposition of insoluble product and loading molecules. Fig. 5 indicates the faradic impedance spectra (Nyquist plot, Z_{im} vs. Z_{re}) in the presence of 5 mM $[Fe(CN)6]^{3-/4-}$ in 0.1 M KCl Solution. The polarization potential applied in impedance measurements was 220 mV vs. Ag/AgCl which was determined from recorded CV curve of redox species. The faradic impedance plot of the bare GC electrode has been shown as a straight line indicating domination of the mass diffusion limiting effect over the electron transfer process. Furthermore, corresponded curve of GC/GO/TiO_2 shows a trouble in charge transferring and a small semi-circle at high frequency is shown for GC/GO/TiO_2-OISL which corresponds to the electron transfer limited process. On the other hand, this modified electrode demonstrates the formation of a much larger semicircle after further modification with GOD, due to the inhibition of the electron transfer to the redox species on the GC/GO/TiO_2-OISL/GOD-electrode.

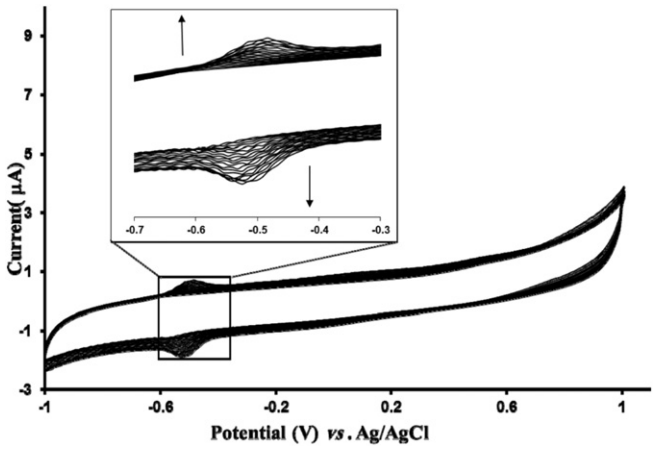

Fig. 2. Consecutive cyclic voltammograms of a GC/GO/TiO_2-IOSL in phosphate buffer solution (pH 7) containing 5 $mg \cdot ml^{-1}$ GOD, scan rate 0.1 V s^{-1}. Inset shows the expanded cyclic voltammogram indicated enzyme immobilization.

3.3. Direct voltammetry of GC/TiO_2-IOSL/GOD-electrode

Electrochemical properties of GC/TiO_2-IOSL/GOD-electrode has been used to investigate the amount of adsorbed GOD. Fig. 6A illustrates the recorded cyclic voltammetry of different electrodes in 0.1 M blank phosphate buffer solution (pH = 7) at 100 mV/s. The GO, GO/TiO_2 and GC/GO-IOSL modified electrodes did not show any obvious redox peak, suggesting that Graphene oxide, TiO_2 and IOSL are electro-inactive in this potential windows. After immobilization of GOD onto GO/TiO_2-IOSL, the GO/TiO_2-IOSL/GOD modified electrode shows a pair of well-known redox peak at −0.465 formal potential, corresponded to direct electron transfer of loaded GOD for the conversion of GOD (FAD) to GOD ($FADH_2$). These potentials are very close to standard electrode potential (0.46 V) for FAD/$FADH_2$ at pH 7 ($T = 25$ °C) [47] indicating successful impregnation of enzyme at IOSL. Since the GO/TiO_2/GOD modified electrode doesn't show any peaks, which may be related to ineffective enzyme immobilization or denaturation of GOD at GO/TiO_2. Thus, the IOSL is very effective in GOD loading as the most GOD molecules retain their native structure after immobilization. On the other hand, the separation of anodic to cathodic peak potentials is 50 mV and ratio of anodic to cathodic peak current is about one. This result indicates that GOD undergoes a quasi-reversible redox process at the surface of organic-inorganic nano-composite. The good electrochemical behaviour of GOD arises from biocompatibility of fabricated nanocomposite with GOD. The biocompatibility of bio-composite should be related to mesoporous structure, conductivity and large number of functional group [48]. The modified electrode was verified by monitoring the remaining amount of active enzyme (GOD) using successive sweeps of cyclic voltammograms, 100 cycles with scan rate of 100 mV s^{-1} in potential range 0.0 to −1 V. (Fig. 6B). The GOD corresponded peak height was almost 96% of its initial value after

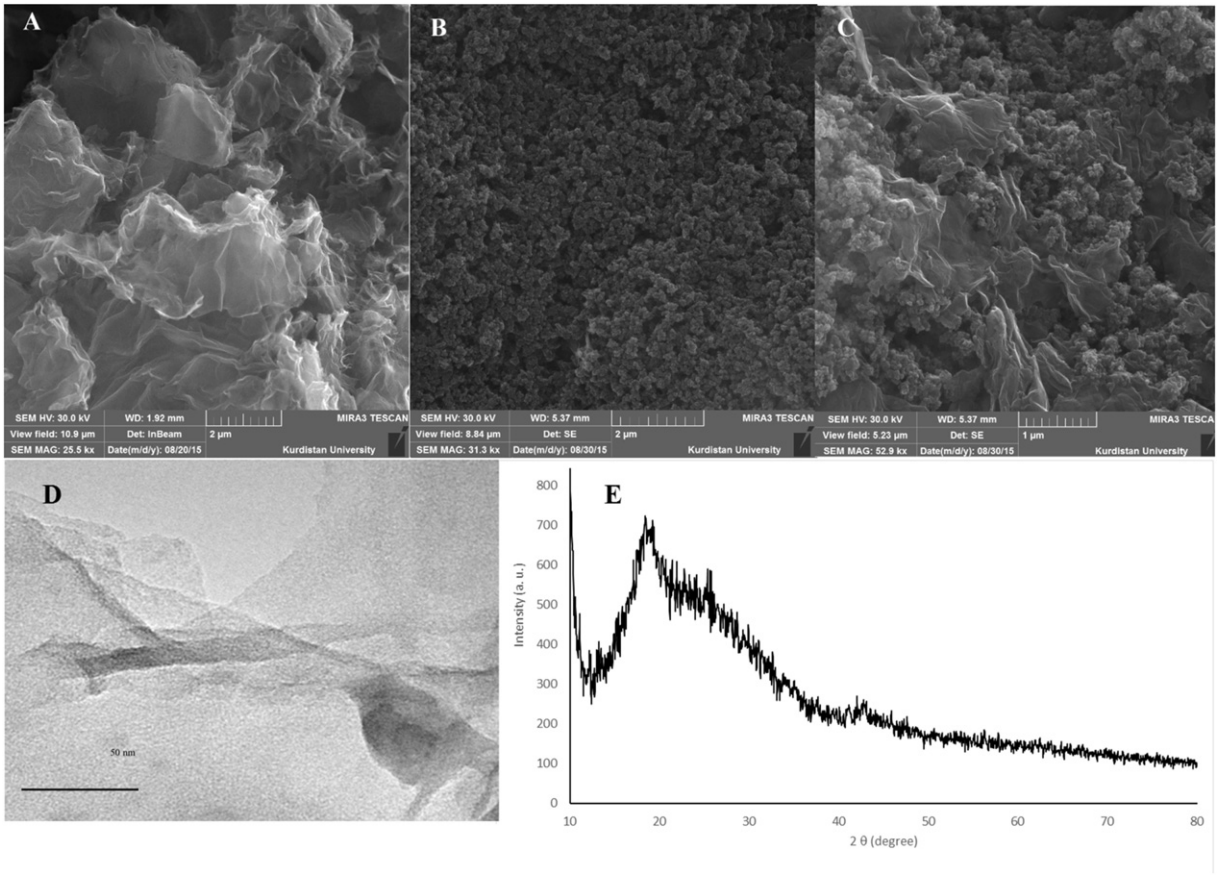

Fig. 3. FE-SEM images of A) Gr_{ox} B) TiO_2 nanoparticles with a particle size 15–20 nm C) and GO/TiO_2 nanocomposite D) TEM image of graphene oxide nanosheet E) XRD pattern of graphene oxide.

100 cycles and peak potential remained nearly unchanged implies to the remaining of GOD on the electrode surface.

Based on our finding, the fabricated Nano-composite has great effect on the kinetics of electrode reaction and provides a suitable environment for the GOD to transfer electron with underlying GC electrode. To obtain the kinetic parameters of GOD at GC/GO-IOSL the effect of the scan rate on the electrochemical response of loaded GOD is shown in Fig. 7A. As it has been shown in inset plot (Fig. 7B), the peak current increase linearly with an increase of the scan rate from 10 to 100 mVs^{-1} ($R^2 = 0.9982$), which indicates that the GOD redox reaction Is a surface-controlled electrochemical process. At scan rate below 100 mVs^{-1} the peak to peak separation is lower than 60 mV, suggesting facial charge transfer kinetics over this range of sweep rate. On the other hand, it is found that the anodic and cathodic peak potential of the immobilized GOD, shifted to positive and negative direction respectively, possibly because of the resistance of the modified layer. As observed in inset for higher scans rate (>2000 mVs^{-1}) the peak to peak separation is proportional to logarithm of scan rate, implied to charge kinetic control process. Based on the Laviron theory, the transfer coefficient (α) and heterogeneous electron transfer rate constant (k_s) can be estimated by measuring the variation of peak potential with scan rate [49]. The following Eqs. (I), (II), (III) and (IV), used to calculate of α and k_s.

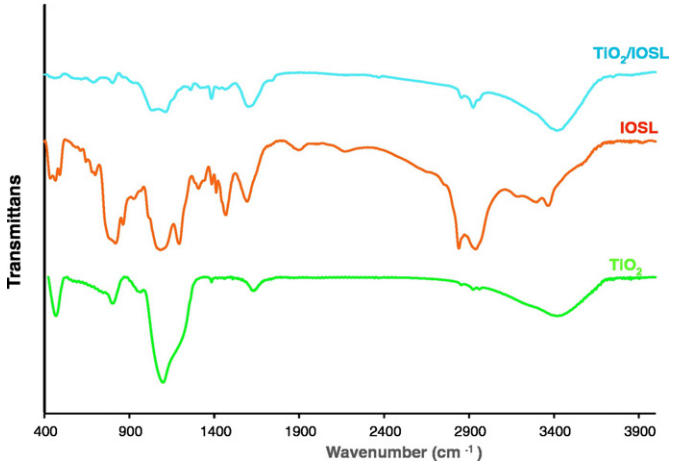

Fig. 4. FTIR spectra of (a) untreated nano-TiO_2, (b) pure IOSL, and (c). OISL-grafted TiO_2 nano-particle.

$$E_c = E^\circ + \frac{RT}{(1-\alpha)nF} \ln\left[\frac{(1-\alpha)}{m}\right] \quad (I)$$

$$E_a = E^\circ + \frac{RT}{\alpha nF} \ln\left[\frac{\alpha}{m}\right] \quad (II)$$

$$\log K_s = \alpha \log(1-\alpha) + (1-\alpha)\log\alpha - \log\left(\frac{RT}{nF\nu}\right) - \frac{\alpha(1-\alpha)nF\Delta E_p}{2.3RT} \quad (III)$$

$$m = \left(\frac{RT}{F}\right)\left(\frac{k_s}{n\nu}\right) \quad (IV)$$

In these equations, m = (RT/F)(ks/nυ), n is the number of electrons transferred, $\nu(Vs^{-1})$ is the scan rate, R, T and F are constants (R = 8.314 J mol − 1 K − 1, T = 298 K, F = 96,485C mol − 1) and E_p is the peak potential. From Fig. 7. the plot of E_p versus log υ yields two straight lines with the slopes of 2.3RT/αn and −2.3RT/(1-α) n for the anodic and cathodic peaks, respectively. Using the slopes of these plots, the values for α and can be estimated as 0.53 and based on Eq.

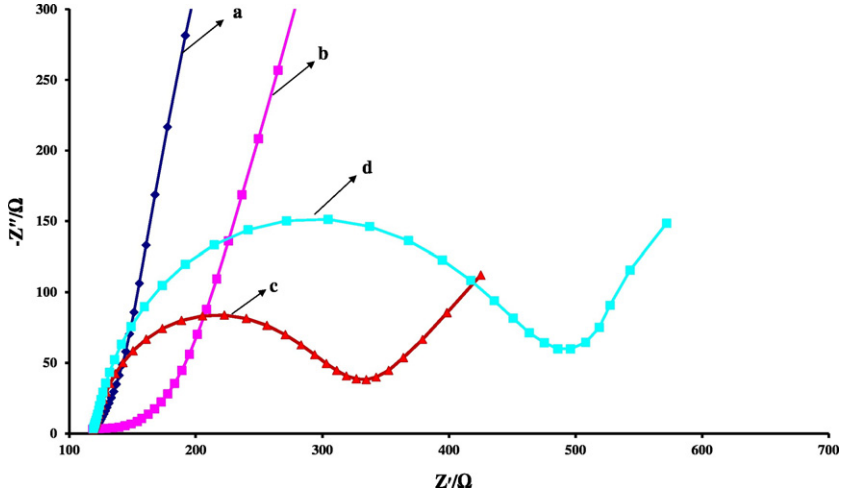

Fig. 5. Nyquist plots of (a) GC, (b) GC/GO/TiO_2, (c) GC/GO/TiO_2-IOSL and (d) GC/GO/TiO_2-IOSL/GOD electrode with supporting electrolyte solution of 5 mM $Fe(CN)_6^{3-/4-}$ and 0.1 M KCl.

(III) and from the values of ΔE_p (for scan rates > 200 mV/s) the average value of ks is determined to be 1.75 ± 0.1 s^{-1}. The obtained k_s value is comparable or greater than the corresponding values observed for GOD immobilized on self-assembled monolayer (0.026 s^{-1}) [50], on CNTs (1.12 s^{-1}) [51] and (1.44 s^{-1}) [52].

For the reversible redox reaction the surface concentration of glucose oxidase (Γ) on the GC/GO/*TiO_2-IOSL* electrode can be approximately calculated from the slope of peak currents vs. scan rate, using eq. (V). Estimated value is 1.23×10^{-9} mol cm^{-2} which suggests the formation of an approximate monolayer of GOD on the surface of the GC/GO/*TiO_2-IOSL* electrode.

$$I_p = n^2 F^2 \frac{\upsilon A \Gamma}{nF\nu} \quad (V)$$

where A is the surface area (0.0314 cm^2) of the modified electrode and other symbols are well known constant. The obtained Γ value for the amount of immobilized glucose oxidase is much larger than that reported for NH_2–TiO_2–CNT/GC (1.50×10–10 mol cm^{-2}) [53], GOx–SWNTs/GC electrode (2.85×10–13 mol cm^{-2}) [54], MSCF/GOD/Nafion-modified GCEs 8.33×10^{-10} mol cm^{-2} [55]. The electrochemical behaviour of GO/TiO_2-IOSL/GOD-modified electrodes shows strong dependence on the pH value. The recorded cyclic voltammograms of modified electrode shows with increasing pH, the formal potential shifts negatively, exhibiting a linear relationship with a slope of 54.1 mV pH^{-1} over a pH range from 2 to 11 (Fig. 8). The pH dependences of peak potential can be expressed as follows:

$$E^{\circ} = -54.1\text{pH} - 0.1058 \quad \left(R^2 = 0.9984\right) \quad (VI)$$

$$\text{GOD (FAD)} + 2e + 2H^+ \rightarrow \text{GOD (FADH}_2\text{)} \quad (VII)$$

This value is close to the theoretical value of −59 mV pH^{-1} at 25 °C for a reversible two proton coupled with two electron redox reaction process (VI) reported previously for immobilized GOD onto nanostructured TiO_2 [56].

4. Electrocatalytic activity of the GC/GO/TiO_2-IOSL/GOD-electrode

4.1. Electrocatalytic activity of modified electrodes toward oxidation and reduction of H_2O_2

Electrocatalytic activity of nano-biocomposite modified electrode was evaluated by recording the cyclic voltammogram of the GC/GO/TiO_2-IOSL/GOD-electrode in the presence of H_2O_2. The results implied considerable electrocatalytic behaviour of GC/GO/TiO_2OISL/GOD electrode toward oxidation and reduction of H_2O_2. Fig. 9A shows the electrocatalytic response of GC/GO/TiO_2-OISL/GOD-electrode toward

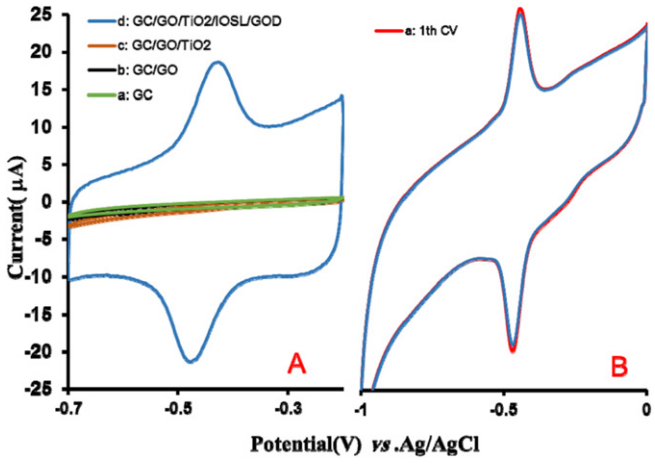

Fig. 6. (A) CVs of glassy carbon electrode in PBS pH 7, scan rate 100 mVs^{-1}, (a) GC/GO, (b) GC/GO/, (c) GC/GO/TiO_2 and (d) GC/IOSL/GOD. (B) The 1st (a) and 100th (b) recorded cyclic voltammograms of modified GC/GO/TiO_2-IOSL/GOD electrode.

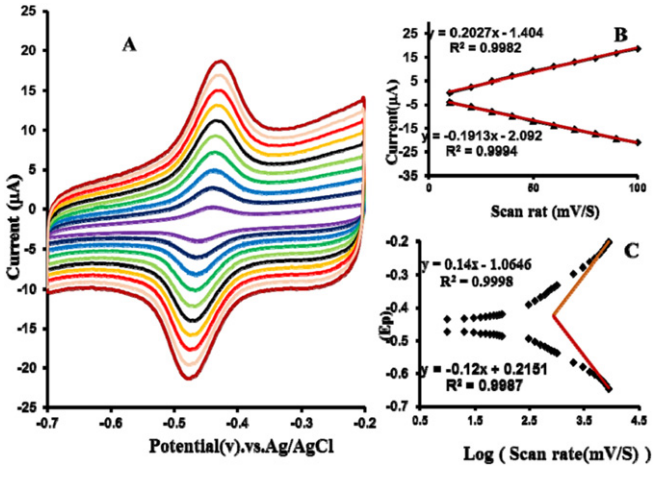

Fig. 7. (A) Cyclic voltammograms of GC/TiO_2-IOSL/GOD electrode at different scan rate in pH 7.0 PBS, From inner to outer, 10, 20, 30, 40, 50, 60, 70, 80, 90 and 100 mVs^{-1}, Insets are plots of anodic and cathodic peak currents vs. scan rate (B), Plot of peak potential separations vs. log (scan rates) (C).

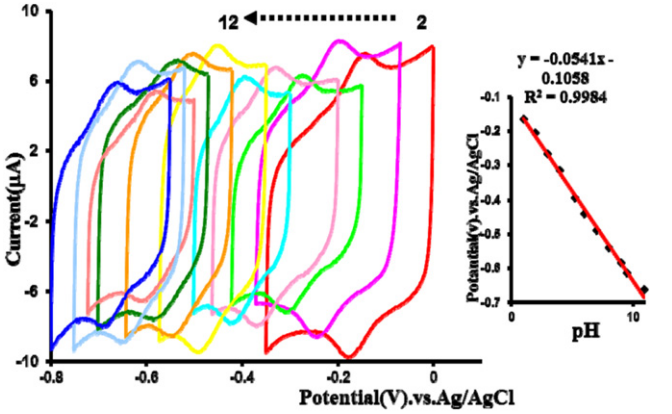

Fig. 8. Recorded cyclic voltammograms of GC/GO/TiO_2-IOSL/GOD modified electrode in different pH solutions, from 2 to 12, scan rate 100 mVs^{-1}. Inset plot of formal potential vs. pH values.

different concentration of H_2O_2 at +0.4 V and −0.25 V (vs. Ag/AgCl) potentials corresponded to electro-oxidation and electro-reduction of H_2O_2 which is explained by following reactions respectively.

$$H_2O_2 \rightarrow 2H^+ + 2e^- + O_2 \quad \text{(VIII)}$$

$$H_2O_2 + 2H^+ + 2e^- \rightarrow 2H_2O \quad \text{(IX)}$$

The activity of TiO_2 toward electro-oxidation of H_2O_2 and the activity of GOD ($FADH_2$/FAD) toward reduction of H_2O_2 are well investigated [57,58]. These two properties can be seen simultaneously in GC/GO/TiO_2-OISL/GOD electrode. The inset plots in Fig. 9B shows the current responses of electrode were recorded for different concentrations of H_2O_2. The catalytic peak currents are proportional to the concentration of H_2O_2 in the range of 2.5 to 17.5 μM. The linear current responses indicate the effective catalytic behaviour of GC/GO/TiO_2-OISL/GOD electrode toward oxidation and reduction of H_2O_2.

4.2. Photo-catalytic activity of GC/GO/TiO_2-OISL/GOD electrode

One of the most unique characteristics of TiO_2 nanoparticles is their optical properties. In presence of light the photoexcited electron-hole pair is generated in the modified TiO_2 nanoparticle. Fig. 10A shows the cyclic voltammograms of GC/GO/TiO_2-OISL/GOD electrode in the dark and under light. As can be seen under light the anodic and cathodic currents are significantly larger than theirs dark currents. On the other hand, the oxidation and reduction over-potential are clearly decreased in the presence light. The larger response current and lower over potentials are good symbols for the biosensors. The following reaction indicates the mechanism for photocatalytic oxidation and reduction of H_2O_2 by fabricated bio-electrode.

$$TiO_2 \xrightarrow{h\nu} e^-_{cb} + h^+_{vb} \quad \text{(X)}$$

$$h^+_{vb} + H_2O_2 \rightarrow O_2 + 2H^+ + 2e \quad \text{(XI)}$$

$$2e^-_{cb} + 2H^+ + H_2O_2 \rightarrow 2H_2O \quad \text{(XII)}$$

The H_2O_2 was oxidized by valance band hole of TiO_2 (hv^+) and the reduction of H_2O_2 catalyzed by conducting bound electron of TiO_2 (cb^-). As a model chronoamperometric technique was used to study the photocatalytic activity of biosensor toward oxidation H_2O_2. Fig. 10B shows the cyclic ON and OFF formation of light induced photocurrent during the oxidation of H_2O_2.

5. Amperometric detection of H_2O_2 at GC/GO/TiO_2-OISL/GOD-electrode

Amperometry under stirred condition used to evaluate the performance of GC/GO/TiO_2-OISL/GOD electrode toward oxidation and reduction of H_2O_2. Fig. 11A shows the steady-state current response H_2O_2 for constant electrode potential of −0.45 and +0.6 V during the successive addition of 1 μM and 20 μM subsequently. It can also be seen that the current response increases (for oxidation) and decreases (for reduction) with increasing H_2O_2 concentration and the calibration plot was linear for concentration range 1 to 120 μM (Fig. 11C). Based on recorded chronoamperogram for addition of 1 μM (Fig. 11B) and also at signal to

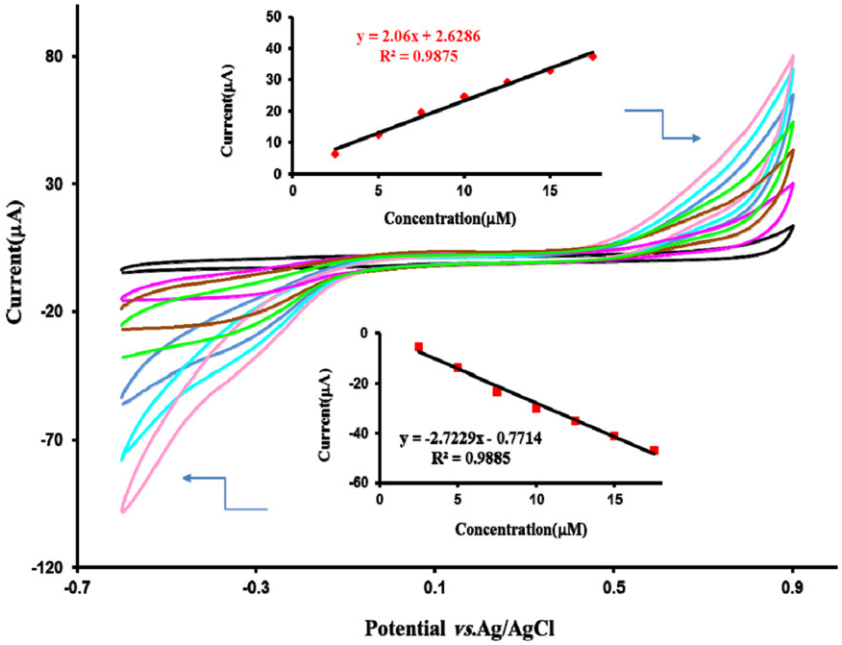

Fig. 9. (A) CVs of GC/GO/TiO_2-OISL/GOD electrode in the presence of different concentrations of H_2O_2 in PBS (pH 7) at 20 mVs^{-1}, from inner to outer 0, 2.5, 5, 7.5, 10, 12.5, 15 and 17.5 mM.

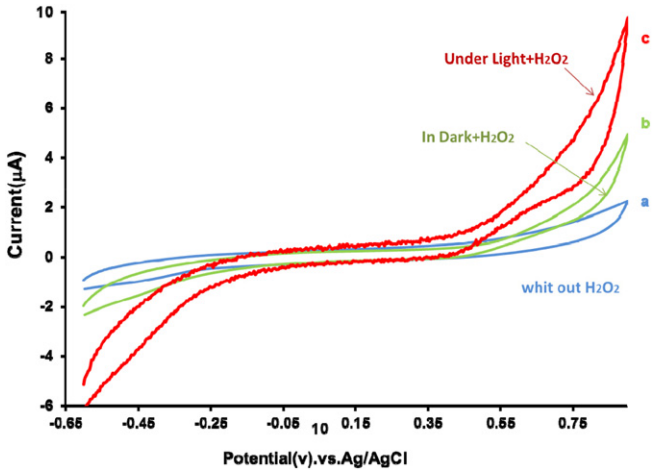

Fig. 10. Cyclic voltamograms of GC/GO/TiO_2-OISL/GOD electrode, PBS (pH 7), at 100 mVs^{-1} (a) in free from H_2O_2, (b) in 1 mM concentration of H_2O_2 in dark and (c) in 1 mM concentration of H_2O_2 under light.

noise of 3, the calculated detection limit for oxidation and reduction of H_2O_2 are 46 and 52 nM, respectively. Also the calculated sensitivity for oxidation and reduction response was 0.33 and 0.35 μA $μM^{-1}$.

6. Photo-enhanced effect of GC/GO/TiO_2-OISL/GOD modified electrode

Amperometric response under stirred condition used to study the photo-induced current response of modified electrode under light illumination. Fig. 11D shows recorded chronoamperogram of GC/GO/TiO_2-OISL/GOD electrode in 1.0 μM H_2O_2 solution, without and under light irradiation at a bias potential of 0.6 V. As can be seen, the photocurrent ascent and descend periodically with light-on and light-off alternatively and the recorded photocurrent is about 2 times higher. The repeatability of photocatalysis response is crucially important in practical application. The cyclic "ON" and "OFF" formation of light-induced photocurrents used to evaluate the repeatability of photocurrent. The results implies to stable and repeatable photocatalytic current.

7. Conclusion

In this work a novel supporting ligand developed to chemically modification of Titanium oxide nanoparticles and effective immobilization of glucose oxidase. FT-IR, and SEM studies used to characterization of modified electrode. The GC/TiO_2-OISL/GOD is stable at least for 3 months when stored at refrigerator. The studies indicate the constructed bio-composite is a biocompatible and helps to prevent the enzyme from denaturation. This enzyme loading method has advantageous when compared to other immobilization procedures such as simple, short immobilization time and good performance for electrocatalytic reduction and oxidation of H_2O_2. The good performance of GC/TiO_2-OISL/GOD electrode indicates this nano-biocomposite is strongly recommended for immobilization of many other enzymes and proteins for fabricating of biosensors and bioelectronics devices. Also, it is expected that the GC/TiO_2-OISL/GOD electrode with good biocompatibility and photocatalytic activity will greatly promote their industrial applications in the enzyme loading and enhancement photocatalytic effect.

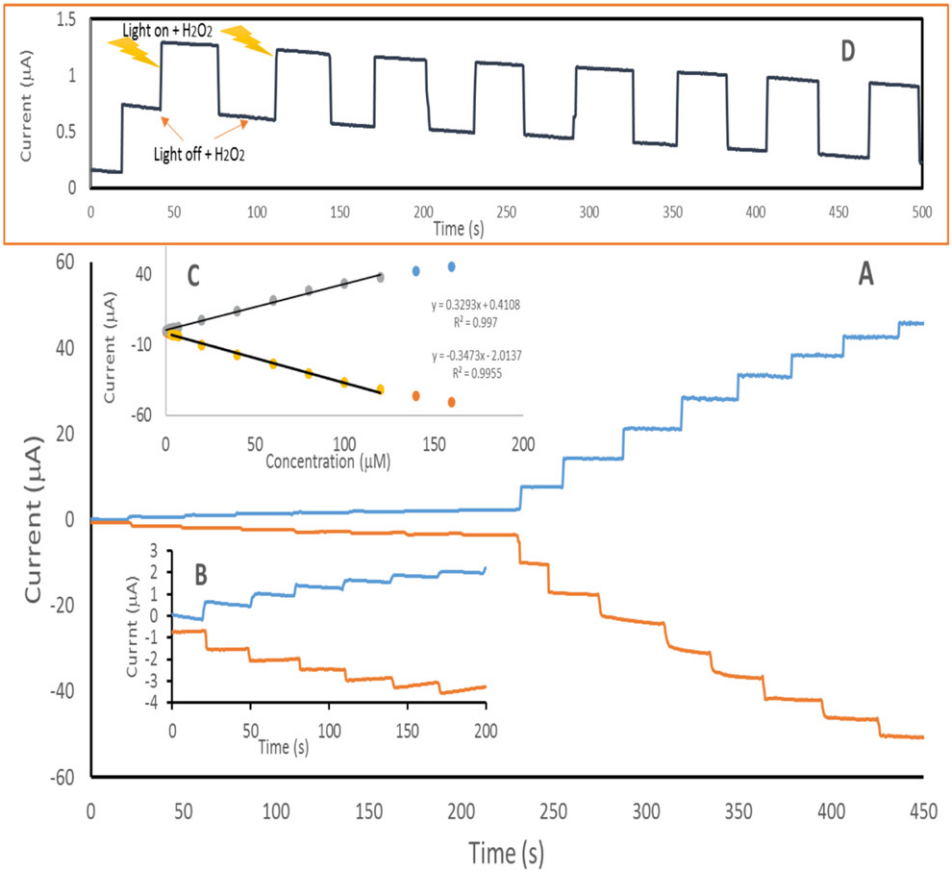

Fig. 11. (A) Amperometric response of rotating GC/GO/TiO_2-OISL/GOD electrode to H_2O_2, conditions −0.45 V and 0.6 V constant potentials, pH 7.0 and rotation speed is 2000 rpm, successive addition of H_2O_2, and corresponded insets plot (C) of chronoamperometric current vs, H_2O_2 concentration. Inset shows the expanded Amperometric response of rotating GC/GO/TiO_2-OISL/GOD electrode to H_2O_2 for addition of 1 μM (B). (D) shows recorded chronoamperogram of GC/GO/TiO_2-OISL/GOD electrode in 1.0 μM H_2O_2 solution, without and under light irradiation at a bias potential of 0.6 V.

Acknowledgments

The financial supports of Nanotechnology Center of Iran and Research Office of Kurdistan University gratefully acknowledged.

References

[1] A. Katsuhiko, J. Qingmin, M. Taizo, N. Masanobu, Y. Yusuke, A. Hideki, P.H. Jonathan, Chem. Soc. Rev. 42 (2013) 6322–6345.
[2] A. Salimi, R. Hallaj, S. Soltanian, Electroanalysis 21 (2009) 2693–2700.
[3] C. Nils, G. Hanna, T. Christian, O. Lisbeth, H. Krister, A. Bjorn, Adv. Colloid Interf. Sci. 205 (2014) 339–360.
[4] K. Sushma, Z. Maogen, G. Waldemar, Anal. Chem. 85 (2013) 1208–1214.
[5] G.L.J. Chunxian, M.L. Chang, L. Yuanyuan, C. Qingbo, H. Xintang, L. Lei, Y. Electrochem. Commun. 11 (2009) 202–205.
[6] D. Han, S. Filocamo, R. Kirby, L.J. Steck, ACS Appl. Mater. Interfaces 3 (2011) 4633–4639.
[7] Y. Jipei, G. Weiwei, W. Erkang, Anal. Chem. 80 (2008) 1141–1145.
[8] H.J. Hecht, D. Schomburg, H. Kalisz, R.D. Schmid, Biosens. Bioelectron. 8 (1993) 197–203.
[9] O. Barbosa, C. Ortiz, Á.B. Murcia, R. Torres, R.C. Rodrigues, R. Fernandez-Lafuente, Biotechnol. Adv. 33 (2015) 435–456.
[10] R. Dicosimo, J. McAuliffe, A.J. Poulose, G. Bohlmann, Chem. Soc. Rev. 42 (2013) 6437–6474.
[11] S. Cantone, V. Ferrario, L. Corici, C. Ebert, D. Fattor, P. Spizzo, L. Gardossi, Chem. Soc. Rev. 42 (2013) 6262–6276.
[12] H. Vaghari, H. Jafarizadeh-Malmiri, M. Mohammadlou, A. Berenjian, N. Anarjan, N. Jafari, S. Nasiri, Biotechnol. Lett. 38 (2016) 223–233.
[13] F. Kazenwadel, M. Franzreb, B.E. Rapp, Anal. Methods 7 (2015) 4030–4037.
[14] R.C. Rodrigues, C. Ortiz, A. Berenguer-Murcia, R. Torres, R. Fernández-Lafuente, Chem. Soc. Rev. 42 (2013) 6290–6307.
[15] C. Garcia-Galan, A. Berenguer-Murcia, R. Fernandez-Lafuente, R.C. Rodrigues, Adv. Synth. Catal. 353 (2011) 2885–2904.
[16] R.C. Rodrigues, Á. Berenguer-Murcia, R. Fernandez-Lafuente, Adv. Synth. Catal. 353 (2011) 2216–2238.
[17] A. Salimi, R. Hallaj, S. Soltanian, Biophys. Chem. 130 (2007) 122–131.
[18] Y. Zhang, H. Wu, X. Huang, J. Zhang, S. Guo, Nanoscale Res. Lett. 6 (2011) 1–7.
[19] A. Salimi, E. Sharifi, A. Noorbakhsh, S. Soltanian, Biosens. Bioelectron. 22 (2007) 3146–3153.
[20] M. Li, S. Dong, N. Li, H. Tang, J. Zheng, RSC Adv. 5 (2015) 14704–14711.
[21] M.N. Tahir, F. Natalio, H.A. Therese, A. Yella, N. Metz, M.R. Shah, E. Mugnaioli, R. Berger, P. Theato, H.C. Schroder, W.E.G. Muller, W. Tremel, Adv. Funct. Mater. 19 (2009) 285–291.
[22] J. Qiu, S. Zhang, H. Zhao, Sensors Actuators B Chem. 160 (2011) 875–890.
[23] B. Christopher Jacobs, M. Jennifer Peairs, B. Jill Venton, Anal. Chim. Acta 662 (2010) 105–127.
[24] S.J. Bao, C.M. Li, J.F. Zang, X.Q. Cui, Y. Qiao, J. Guo, Adv. Funct. Mater. 18 (2008) 591–599.
[25] P. Benvenuto, A.K.M. Kafi, J. Electroanal. Chem. 627 (2009) 76–81.
[26] H.F. Cui, K. Zhang, Y.F. Zhang, Y. Sun, J. Wang, W.D. Zhang, J.H.T. Luong, Biosens. Bioelectron. 46 (2013) 113–118.
[27] Z.D. Gao, F.F. Guan, C.Y. Li, H.F. Liu, Y.Y. Song, Biosens. Bioelectron. 41 (2013) 771–775.
[28] J. Davis, K.S. Coleman, B. Azamian, C. Bagshaw, M. Green, Chem. Eur. J. 9 (2003) 3732–3739.
[29] J. Wu, M. Xu, G. Zhao, Electrochem. Commun. 12 (2010) 175–177.
[30] S. Liu, A. Chen, Langmuir 21 (2005) 8409–8413.
[31] C.J. Campbell, A.E.G. Cass, J.R. Durrant, Langmuir 17 (2001) 7899–7906.
[32] A. Heller, B. Feldman, Chem. Rev. 108 (2008) 2482–2505.
[33] F.P. Pereira, R.M.B.O. Duarte, A.C. Duarte, Trends Anal. Chem. 40 (2012) 90–105.
[34] A. Sassolas, L.J. Blum, B.D.L. Bouvier, Biotechnol. Adv. 30 (2012) 489–511.
[35] X.J. Huang, P.C. Chen, F. Huang, Y. Ou, M.R. Chen, Z.K. Xu, J. Mol. Catal. B Enzym. 70 (2011) 95–100.
[36] K.R. Jegannathan, L. Jun-Yee, E.S. Chan, O.P. Ravindra, Fuel 89 (2010) 2272–2277.
[37] A. Salimi, A. Noorbakhsh, Electrochim. Acta 56 (2011) 6097–6105.
[38] I.A. Siddiquey, E. Ukaji, T. Furusawa, M. Sato, N. Suzuki, Mater. Chem. Phys. 105 (2007) 162–168.
[39] C.P. Sousa, A.S. Polo, R.M. Torresi, S.I. Cordoba de Torresi, W.A. Alves, Adv. Colloid Interf. Sci. 346 (2010) 442–447.
[40] C. Leger, P. Bertrand, Chem. Rev. 108 (2008) 2379–2438.
[41] F. Nasiri, A. Zolali, M. Ahmadiazar, Phosphorus Sulfur Silicon Relat. Elem. 189 (2014) 180–184.
[42] S. Mallakpour, A. Barati, Prog. Org. Coat. 71 (2011) 391–398.
[43] D.C. Marcano, D.V. Kosynkin, J.M. Berlin, A. Sinitskii, Z. Sun, A. Slesarev, L.B. Alemany, W. Lu, J.M. Tour, ACS Nano 8 (2010) 4806–4814.
[44] S. Stankovich, D.A. Dikin, R.D. Piner, K.A. Kohlhaas, A. Kleinhammes, Y. Jia, Y. Wu, S.T. Nguyen, R.S. Ruoff, Carbon 45 (2007) 1558–1565.
[45] E. Ukaji, T. Furusawa, M. Sato, N. Suzuki, Appl. Surf. Sci. 254 (2007) 563–569.
[46] J. Liu, M.N. Paddon-Row, J.J. Gooding, J. Phys. Chem. B 108 (2004) 8460–8466.
[47] A. Katsuhiko, J.P.H. Qingmin Ji, Macromol. Biosci. 8 (2008) 981–990.
[48] E. Laviron, J. Electroanal. Chem. 101 (1979) 19–28.
[49] L. Jiang, C.J. McNeilb, J.M. Cooper, J. Chem. Soc. Chem. Commun. 12 (1995) 1293–1295.
[50] M.V. Jose, S. Marx, H. Murata, R.R. Koepsel, A.J. Russell, Carbon 50 (2012) 4010–4020.
[51] H.Z. Zhao, J.J. Sun, J. Song, Q.Z. Yang, Carbon 48 (2010) 1508–1514.
[52] M. Tasviri, H.A. Rafiee Pour, H. Ghourchian, M.R. Gholami, J. Mol. Catal. B Enzym. 68 (2011) 206–210.
[53] Q. Liu, X. Lu, J. Li, X. Yao, J. Li, Biosens. Bioelectron. 22 (2007) 3203–3209.
[54] S. Wu, H.X. Ju, Y. Liu, Adv. Funct. Mater. 17 (2007) 585–592.
[55] S.J. Bao, C.M. Li, J.F. Zang, X.Q. Cui, Y. Qiao, J. Guo, Adv. Funct. Mater. 18 (2008) 591–599.
[56] M.N. Romanias, A.E. Zein, Y.J. Bedjanian, Phys. Chem. A 116 (2012) 10.
[57] X. Shu, Y. Chen, H. Yuan, S. Gao, D. Xiao, Anal. Chem. 79 (2007) 3695–3702.
[58] M.A. Kausaite, V. Mazeiko, A. Ramanaviciene, Y. Oztekin, A.O. Solak, A. Ramanavicius, Electroanalysis 26 (2014) 1528–1535.